Modeling transport across the running-sandpile cellular automaton by means of fractional transport equations

R. Sánchez,[1,*] D. E. Newman,[2] and J. A. Mier[3]

[1]*Departamento de Física, Universidad Carlos III de Madrid, 28911 Leganés, Madrid, Spain*
[2]*Department of Physics, University of Alaska, Fairbanks, Alaska 99775-5920, USA*
[3]*Departamento de Física Aplicada, Universidad de Cantabria, 39005 Santander, Spain*

Fractional transport equations are used to build an effective model for transport across the running sandpile cellular automaton [Hwa *et al.*, Phys. Rev. A **45**, 7002 (1992)]. It is shown that both temporal and spatial fractional derivatives must be considered to properly reproduce the sandpile transport features, which are governed by self-organized criticality, at least over sufficiently long or large scales. In contrast to previous applications of fractional transport equations to other systems, the specifics of sand motion require in this case that the spatial fractional derivatives used for the running sandpile must be of the completely asymmetrical Riesz-Feller type. Appropriate values for the fractional exponents that define these derivatives in the case of the running sandpile are obtained numerically.

I. INTRODUCTION

Sandpile cellular automata became the poster child for self-organized criticality (SOC) from the very early days [1], and many variants have been constructed to provide simplified frameworks in which the complex dynamics of many different systems could be studied, from earthquakes to forest fires and from solar flares to accretion disks [2–8] (although, curiously enough, it has been proven [9,10] that these automata do not provide a good description of natural sandpile dynamics). All of these automaton variants contain, in one way or another, the main ingredients needed for SOC dynamics to appear: an open, driven system with a local instability threshold and a large separation of scales between local drive and instability relaxation. The resulting dynamic steady state, once the external drive and sandpile losses are balanced on average, is known as the SOC state [1]. It exhibits properties typical of critical points such as scale invariance, long-term memory, and divergent correlations. Transport through the system is inherently bursty and of nondiffusive nature, being dominated by avalanches.

In the field of magnetically confined fusion (MCF) toroidal plasmas, a variant of the sandpile automaton known as the running sandpile [11–14] has been used extensively to try to understand turbulent transport characteristics in tokamaks and stellarators [15]. A main feature of the running sandpile, which somewhat moves it away from other sandpile automata often discussed in the literature, is that the separation between the timescales of drive and relaxation is finite and, sometimes, not very large. This comes about because, in contrast to the standard sandpile automaton, the drive is not stopped once an avalanche starts and reactivated after all avalanching activity dies away. Instead, the sandpile keeps on being driven as avalanches progress in time. This choice of rules

makes both analytical progress and numerical characterization of avalanches more challenging (avalanches do overlap, for instance) but, at the same time, introduces a timescale in the problem that is essential for many practical applications and, in particular, in the context of MCF plasmas [15–17].

Among the many needs of the MCF tokamak program, an important one is the development of effective mean-field transport models with reliable predictive capabilities regarding the confinement of the plasma density and energy in these toroidal traps [18]. Several authors have suggested that, at least in those plasma regimes in which SOC-like dynamics appear to dominate radial transport, these effective models would require the use of fractional transport equations [15,19–23]. In this article, we describe in detail how one such effective transport model could be built for the running sandpile cellular automaton, given its role as a simple, but still meaningful, paradigm for the transport dynamics taking place in MCF plasmas while in a SOC-like regime. The results reported here, albeit meaningful in their own right within the context of the study of sandpile automata, might also teach some useful lessons regarding the construction of effective models in MCF plasmas, as well as for any other natural systems with similar directed transport dynamics.

The article is thus organized as follows: in Sec. II the running sandpile automaton is briefly introduced. Then, an effective transport equation is built for the running sandpile in Sec. III starting from a continuous-time random walk (CTRW) model that incorporates the most salient features of transport in the sandpile. The resulting effective transport equation contains both fractional derivatives in space and time. The most relevant free parameters that define the fractional transport model, namely its fractional exponents, are then quantified numerically in Sec. IV, with the help of tracers (i.e., marked grains of sand). We will then proceed to discuss the meaning of these results in Sec. V and draw some final conclusions in Sec. VI.
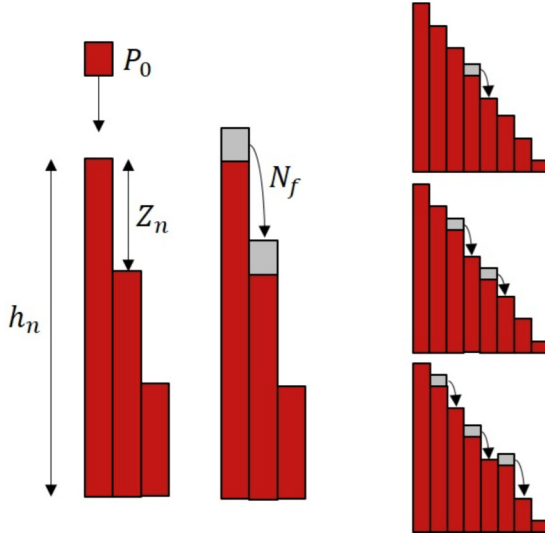
─────────
*Corresponding author: raul.sanchez@uc3m.es

FIG. 1. Left: Sketch of the one-dimensional sandpile in real space explaining the corresponding automaton rules. Right: Sketch of an avalanche taking place.

FIG. 2. Plot of the average sandpile slope, $-\langle Z \rangle$, vs the estimate $-(Z_c - N_f/2)$ for two sandpiles with lengths $L = 100$ [in red (dark gray) squares] and $L = 300$ [in green (light gray) circles] and various values of N_F and Z_c. The error bars represent the standard deviation that naturally scales with N_F.

II. THE RUNNING SANDPILE MODEL

The sandpile celluar automaton that we will consider in this paper is the one-dimensional, driven, and directed running sandpile [11,12] (see Fig. 1). The sandpile domain consists of L cells or sites, numbered from $n = 1$ to $n = L$. To each cell n, a variable h_n is assigned that represents the amount of sand stored (or its height) in the cell.

The running sandpile state is evolved in time in the following way. First, by randomly dropping N_b grains of sand on every cell at each iteration with a probability P_0. What happens next depends on the value of the local slope at each of the sandpile cell. A critical slope exists, $-Z_c$ ($Z_c > 0$), that, when locally overcome (i.e., when the local gradient $Z_n = h_{n+1} - h_n$ exceeds $-Z_c$), causes the removal of N_f grains of sand to the adjacent position. All cells are checked for instability once per iteration. After this is done, a new iteration starts, and new sand is randomly dropped over the sandpile cells. The rules of the running sandpile are completed by imposing a closed boundary condition at $n = 1$, so that no sand flux enters that cell from the left, and an open boundary condition at $n = L$, so that all sand grains reaching the bottom edge of the sandpile (in chunks of N_f, since they must be transported by avalanches; rain is not added to the last cell) are removed from the system.

The SOC character of the sandpile transport dynamics is rooted in the existence of this critical slope. In addition, it is also important that the relaxation process has some inertia. That is, that $N_f > N_b$, to avoid the average slope staying at the critical value $-Z_c$ all the time. Also, it must happen that $N_f > P_0 N_b L$ in order to avoid the sandpile becoming overdriven. The reason for this condition is that, since the sandpile receives $P_0 N_b L$ grains of sand per iteration (on average), steady state requires this value to be less than what can be extracted at the sandpile edge per iteration, given by N_f.

The running sandpile will always reach a steady state under a continuous, fixed-average external drive. The average slope of the sandpile, at steady state, is roughly given by
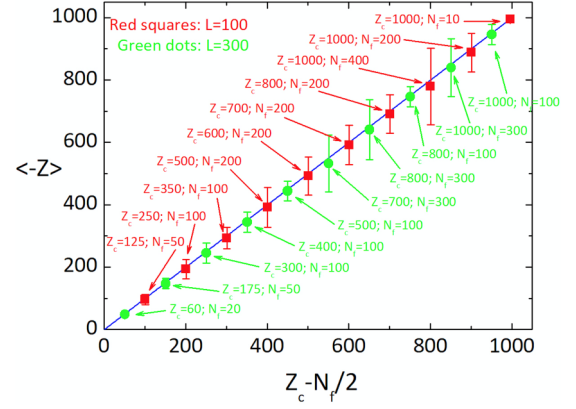
$\bar{Z} \simeq -(Z_c - N_f/2)$ due to the aforementioned inertia of the relaxation (see Fig. 2; an explicit estimation of the average slope in the running sandpile is given, for instance, in Ref. [24]; an alternative estimation is provided in Ref. [25]). Transport across the sandpile domain will be driven by avalanches, that exhibit an approximately self-similar distribution of linear sizes and durations over an extended range of scales (or *mesorange*) that is limited only by finite size effects [12]. Avalanche initiation points are roughly uniformly distributed throughout the pile, except at the very edge, where the open boundary condition imposes a larger mean slope. The probability of an avalanche stopping increases with the cell index, n, due to the fact [25] that the sand that needs to be transported down the slope must increase to balance the integrated drive over all cells $n' < n$. Furthermore, the time series of the sandpile activity, defined as the number of unstable cells at each time, exhibits long-term persistence over scales much longer than the maximum avalanche duration [12,26]. In particular, persistence in the running sandpile has been extensively studied using, among other methods, its power spectrum (that scales as f^{-a}, $0 < a < 1$ over the SOC mesorange) or determining its Hurst exponent (that satisfies $H > 0.5$ over the SOC mesorange timescales).

In order to characterize the particle confinement in the sandpile from a global perspective, it is useful to measure the average time taken for a marked grain of sand to move across the whole sandpile and reach the edge. We will later describe in detail how these marked grains are advanced (see Sec. IV). For now, it suffices to say that their average confinement time τ_c has been estimated using a large number of marked grains and then fit to a product of powers of the main sandpile parameters. Namely, the sandpile length L, the number of grains locally moved when unstable N_f, the number of grains dropped on every cell at each iteration N_b, and the rain probability P_0 [the critical threshold Z_c does not affect the confinement time; it has been set to $Z_c = 200$ in all simulations). The resulting global scaling for τ_c is (see also, Fig. 3)

$$\tau_c = 0.34 L^{0.4} N_f (N_b P_0)^{-1}. \tag{1}$$

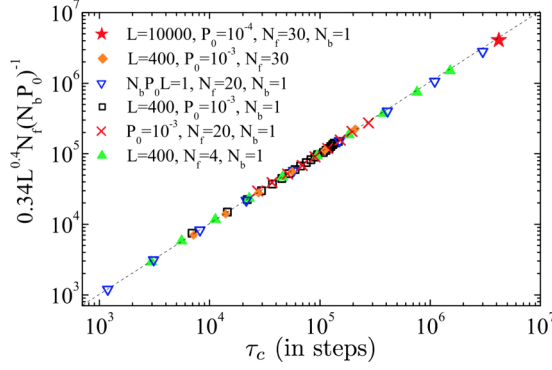FIG. 3. Global scaling of the mean value of the transit time (τ_c) with sandpile parameters L, N_f, N_b, and P_0.

Clearly, the most remarkably feature of this global scaling law, which reveals its nondiffusive (i.e., avalanche) dynamics, is the value of the L exponent.

III. MEAN-FIELD TRANSPORT MODEL FOR THE RUNNING SANDPILE AUTOMATON IN TERMS OF FRACTIONAL DERIVATIVES

In this section, we will construct an effective mean-field transport model for the running sandpile just described. The starting point is the well-known CTRW formalism [27] that we have adapted to the reality of transport in the running sandpile automaton. The effective transport model results from considering the long-time, large-distance asymptotic behavior of this CTRW, as it has traditionally been done for many other problems [28]. In the one-dimensional CTRW, a number of walkers N are considered. Each walker stays at its initial position, x_0, for a *waiting time* Δt. Then, it carries out a *jump* of size Δx, that takes the walker to its new position, $x_0 + \Delta x$. This process is carried out many times by each walker. The CTRW is defined, naturally, by prescribing the pdf of both jump sizes, $p(\Delta x)$, and waiting times, $\psi(\Delta t)$. In a purely diffusive system, the transport process is expected to have finite characteristic scales, both in time and space (in a gas, for instance, these scales could be the mean free path and the inverse collision frequency, respectively). In a SOC system, however, the self-similar, critical nature of the SOC state prevents these characteristic scales from existing. The choices for p and ψ must then naturally reflect these features, as will be discussed soon. These waiting times will endow the CTRW with an interesting property that is sometimes referred to as a "semi-Markovian" character. Namely, it refers to the fact that in spite of the waiting times being identically distributed and independent random variables, their accumulation introduces a memory in the absence of a finite first moment and thus non-Markovian properties [29].

Before getting any deeper into that discussion, it is, however, convenient to solve the CTRW. By that, we mean to calculate its propagator, $G(x,t|x_0,t_0)$, as a function of the choices made for $p(\Delta x)$ and $\psi(\Delta t)$. The propagator simply gives the probability of finding one walker at position x and time t, assuming it was at position x_0 at a previous time t_0. Once known, the general solution of the CTRW can be written, for arbitrary initial (i.e., $t = 0$) walker density, $n_0(x)$, and external source of walkers,

$S(x,t)$, as

$$n(x,t) = \int_{-\infty}^{\infty} dx' G(x,t|x',0) n_0(x')$$
$$+ \int_0^t dt' \int_{-\infty}^{\infty} dx' G(x,t|x',t') S(x',t'). \quad (2)$$

By defining an augmented source as $S^{\mathrm{aug}}(x,t) = S(x,t) + n_0(x)\delta(t)$, we can recast this equation as

$$n(x,t) = \int_0^t dt' \int_{-\infty}^{\infty} dx' G(x,t|x',t') S^{\mathrm{aug}}(x',t'). \quad (3)$$

Since the CTRW is invariant under translations in both space and time (or, in other words, since the pdfs p and ψ do not explicitly depend on the position x of the walker or the current time t), it then follows that the propagator only depends on the relative distance and the elapsed time, which turns Eq. (3) into

$$n(x,t) = \int_0^t dt' \int_{-\infty}^{\infty} dx' G(x - x', t - t') S^{\mathrm{aug}}(x',t'). \quad (4)$$

This double convolution combines well with the fact that the propagator of the CTRW can straightforwardly be found in Fourier-Laplace space, as shown in Ref. [27]. It is given by

$$\bar{G}(k,s) = \frac{(1 - \tilde{\psi}(s))/s}{1 - \tilde{\psi}(s)\hat{p}(k)}. \quad (5)$$

Here, s and k respectively stand for the Laplace and Fourier variables related to Δt and Δx. The Laplace transform is represented by a tilde on top of the function being transformed, the Fourier transform by a hat, and the double Laplace-Fourier transform by a bar.

A mean-field transport model can now be built by first proposing suitable choices for $p(\Delta x)$ and $\psi(\Delta t)$ and then keeping just the long-time, large-distance asymptotic behavior of the resulting propagator. In Fourier-Laplace space, this means taking the asymptotic behavior for $k \to 0$ and $s \to 0$. For instance, the classical diffusive equation is obtained [28] by choosing p and ψ to be, respectively, a Gaussian (with zero mean and variance σ^2) and exponential pdf (with mean time τ_0). The Gaussian law satisfies that

$$\hat{p}(k) \sim 1 - \sigma^2 k^2, \quad k \to 0, \quad (6)$$

and the exponential pdf that

$$\tilde{\psi}(s) \sim 1 - \tau_0 s, \quad s \to 0. \quad (7)$$

This leads to an asymptotic behavior of the propagator of the form,

$$\bar{G}(k,s) \sim \frac{1}{s + (\sigma^2/\tau_0)k^2}, \quad s \to 0, k \to 0. \quad (8)$$

Inserting this expression into Eq. (3), one can easily reorder terms and get

$$s\bar{n}(k,s) - \hat{n}_0(k) \simeq -\frac{\sigma^2}{\tau_0} k^2 \bar{n}(k,s) + \bar{S}(k,s), \quad (9)$$

whose Laplace-Fourier inverse becomes the usual diffusive equation:

$$\frac{\partial n}{\partial t} = \frac{\sigma^2}{\tau_0} \frac{\partial^2 n}{\partial x^2} + S(x,t), \quad n(x,0) = n_0(x). \quad (10)$$

It should be noted that, in the purely diffusive case, σ and τ_0 provide the finite characteristic scales for transport. For that reason, one must choose functions for $p(\Delta x)$ and $\psi(\Delta t)$ that respectively lack a finite variance and a finite mean if the intention is to build a transport model for a system in which the dynamics are self-similar and divergent. The same central limit that advises picking Gaussians in many situations points us now towards strictly stable Lévy distributions $L_{[\alpha,\lambda,\sigma]}(x)$ (see Appendix A), all of which lack a finite variance [30]. The parameter $\alpha \in (0,2)$ determines the tail behavior of the distribution, that scales as $L(x) \sim |x|^{-(1+\alpha)}$ for large values of the argument. Since $\alpha < 2$, all Lévy pdfs do lack a finite variance as stated (in fact, for $\alpha \leqslant 1$, they also lack a finite mean). Next, $\lambda \in [-1,1]$ is a symmetry parameter, with the Lévy law being symmetric [i.e., $L(-x) = L(x), \quad \forall x$] only for $\lambda = 0$. σ, on the other hand, is a shape parameter that measures the width of the distribution in the sense that its finite moments ($p < \alpha$),

$$\langle |x|^p \rangle := \int_{-\infty}^{\infty} dx\, L_{[\alpha,\lambda,\sigma]}(x)|x|^p = c_{\alpha,\lambda}^p(p)\sigma^p, \qquad (11)$$

are proportional to powers of σ. The definition of the constant $c_{\alpha,\lambda}(p)$ can be found elsewhere [30]. For symmetric Lévy pdfs (i.e., those with $\lambda = 0$), one can even define an effective width w by means of the expression $w^p := \langle |x|^p \rangle$.

In many applications [22], the microscopic transport process is unbiased and symmetric in space, that leads to the natural choice of $p(\Delta x) = L_{\alpha,0,\sigma}(\Delta x)$ as the jump size distribution, for some appropriate values of $\alpha < 2$ and $\sigma > 0$ that must be determined. On the other hand, waiting times can only be positive and must therefore lack a finite mean if a characteristic scale does not exist. It is thus convenient to choose $\psi(\Delta t) = L_{\beta,1,\tau}(\Delta t)$ as waiting-time pdf, for appropriate $\beta < 1$ and $\tau > 0$. Distributions with $\beta = 1$ are part of a subfamily known as extremal Lévy distributions (see Appendix A), that have the nice property of being defined only for $\Delta t > 0$. Extremal Lévy pdfs also lack a finite mean since they scale as $\psi(\Delta t) \sim \Delta t^{-(1+\beta)}$ for large Δt.

In the case of the running sandpile automaton, however, sand can only travel in one direction: down the slope. Thus, a symmetric Levy pdf would be an inappropriate choice for the jump pdf. Instead, we will choose another extremal distribution, $p(\Delta x) = L_{\alpha,1,\sigma}(\Delta x)$, with $0 < \alpha < 1$ and $\sigma > 0$. This fully asymmetric choice will, however, lead to a transport equation that is rather different from what is often used in other applications, as it will become apparent very soon. In particular, it is worth to differentiate from other nonsymmetric choices sometimes found in the literature, such as the consideration of CTRWs with a drift [31] that are not adequate for the sandpile case examined here.

To proceed with the derivation of the effective transport model, we will need to use two well-known properties of all extremal Levy distributions [30]; namely that their Laplace transform behaves as

$$\tilde{L}_{[\beta,1,\tau]}(s) \sim 1 - \frac{\tau^\beta s^\beta}{\cos(\pi\beta/2)}, \quad s \to 0, \qquad (12)$$

and that its Fourier transform behaves, for $k \to 0$, as ($i = \sqrt{-1}$)

$$\hat{L}_{[\alpha,1,\sigma]}(k) \sim 1 - \sigma^\alpha |k|^\alpha \left[1 - \frac{ik}{|k|}\tan\left(\frac{\pi\alpha}{2}\right)\right]. \qquad (13)$$

Inserting these asymptotic behaviors into the CTRW propagator [Eq. (5)], one obtains ($s \to 0, k \to 0$):

$$\bar{G}(k,s) \sim \frac{s^{\beta-1}}{s^\beta + \cos\left(\frac{\pi\beta}{2}\right)\frac{\sigma^\alpha}{\tau^\beta}|k|^\alpha\left[1 - \frac{ik}{|k|}\tan\left(\frac{\pi\alpha}{2}\right)\right]}. \qquad (14)$$

The Laplace-Fourier transform of the CTRW general solution [Eq. (3)] then becomes, after some straightforward reordering,

$$s\bar{n}(k,s) - \hat{n}(k,0)$$
$$\simeq \bar{S}(k,s) - s^{\beta-1}\left\{D_{\alpha,\beta}|k|^\alpha\left[1 - i\frac{k}{|k|}\tan\left(\frac{\pi\alpha}{2}\right)\right]\right\}\bar{n}(k,s), \qquad (15)$$

where we have defined a fractional transport coefficient $D_{\alpha,\beta} := \cos(\pi\beta/2)\sigma^\alpha/\tau^\beta$. This equation can be Fourier-Laplace inverted to yield

$$\frac{\partial n}{\partial t} = {_0}D_t^{1-\beta}\left[D_{\alpha,\beta}\frac{\partial^{\alpha,1}n}{\partial|x|^{\alpha,1}}\right] + S(x,t), \qquad (16)$$

by introducing a Rieman-Liouville fractional derivative (see Appendix B) in time and a Riesz-Feller fractional derivative (see Appendix C) in space. In particular, ${_0}D_t^{1-\beta}$ is a Rieman-Liouville fractional derivative of order $1 - \beta$ and start point at $t = 0$. On the other hand, $\partial^{\alpha,1}/\partial|x|^{\alpha,1}$ is a completely asymmetrical (and left-sided) Riesz-Feller fractional derivative of order α.

It is at this point where the most meaningful difference with systems in which unbiased, symmetric transport takes place at the microscopic level. In the unbiased case, one usually picks $p(\Delta x) = L_{\alpha,0,\sigma}(\Delta x)$ as the jump size distribution, which leads to the transport equation [28],

$$\frac{\partial n}{\partial t} = {_0}D_t^{1-\beta}\left[D_{\alpha,\beta}\frac{\partial^\alpha n}{\partial|x|^\alpha}\right] + S(x,t), \qquad (17)$$

which contains the symmetric Reisz operator (Appendix C). As a result, changes in $n(x,t)$ at location x is calculated by collecting the contributions from all locations $x' \langle x$ and $x' \rangle x$. In contrast, Eq. (16) contains the asymmetrical (left-sided) Reisz-Feller derivative, which is defined as

$$\frac{\partial^{\alpha,1}n}{\partial|x|^{\alpha,1}} \propto \frac{d^k}{dx^k}\left[\int_{-\infty}^{x}\frac{n(x')dx'}{(x-x')^{\alpha-k+1}}\right], \qquad (18)$$

with k defined as the integer satisfying $k - 1 < \alpha < k$. Here only points $x' < x$ contribute to the integral, a reflection of the fact that net transport can only come from the left (i.e., down the slope, in the running sandpile) and not from the right.

Furthermore, these distinctions imply that some usual associations made in the context of Eq. (17) are no longer true. For instance, it is traditional to define a transport exponent, $H = \beta/\alpha$, that quantifies how the finite moments of the propagator of Eq. (17) grow with time:

$$\langle |x - x_0|^p G_{\text{Eq. 17}}(x,t|x_0,0) \rangle \propto t^{pH}, \qquad (19)$$

being x_0 the initial position. For unbiased, symmetric motion, $H > 1/2$ is often referred to as superdiffusive behavior, while $H < 1/2$ is subdiffusive behavior. These names reflect the fact that the propagator spreads faster or slower than their diffusive counterpart (i.e., $\beta = 1$, $\alpha = 2$). For biased motion, on the other hand, an exponent $H = \beta/\alpha$ could still be defined, but

it would make no sense to interpret it in a similar way, since the propagator is now fully asymmetric. Therefore, Eq. (19) no longer characterizes how the propagator spreads around its "center of mass," since they will be strongly affected by how fast the "center of mass" itself moves down the slope (which, for symmetric motion, it does not).

IV. FRACTIONAL EXPONENTS FOR THE RUNNING SANDPILE

In order to use Eq. (16) as a mean-field model for transport in the sandpile, we need to estimate first the fractional exponents α and β. There are several ways to do this. One of the simplest ones is to take advantage of the asymptotic behavior of the propagator of the transport equation defined in Eq. (14). In particular, it can be shown that, for fixed t_c, it satisfies that [32]:

$$G(x, t_c|x_0) \sim (x - x_0)^{-(1+\alpha)}, \quad x - x_0 \gg D_{\alpha,\beta}^{1/\beta} t_c^{\beta/\alpha}. \quad (20)$$

On the other hand, for fixed $x_c > x_0$, it satisfies that

$$G(x_c, t|x_0, 0) \sim t^\beta, \quad t \ll D_{\alpha,\beta}^{1/\beta} x_c^{\alpha/\beta}, \quad (21)$$

and

$$G(x_c, t|x_0, 0) \sim t^{-\beta}, \quad t \gg D_{\alpha,\beta}^{1/\beta} x_c^{\alpha/\beta}. \quad (22)$$

Therefore, one can estimate α and β by constructing the propagator of transport in the running sandpile and quantifying how it changes at fixed position and time. How can one estimate this propagator, though? In our case, we do it by introducing tracers in the sandpile.

A. Advancing tracers in the running sandpile

The propagator of the CTRW gave the probability of finding a walker at position x and time t after having been at x_0 at time t_0. The propagator of the transport equation, on the other hand, gives the temporal evolution of the initial condition $n(x, 0) = \delta(x - x_0)$. Therefore, one can in principle estimate it by following the motion of a sufficiently large number of marked grains of sand (or tracers) that are initially localized very close to each other. In order to do this, we need to consider, however, a different population of sand grains that, although advanced together with the normal sand, are inert in the sense that they are not considered when a cell is checked for instability. Or, in other words, none of these tracers are considered when updating the local sandpile height or gradient.

Following Ref. [28], we will focus on a narrow strip of width N_f at the sandpile surface, which is the active layer where motion takes place. We will consider N marked grains of sand that will be initially located close to the center of the sandpile. The temporal evolution of the marked population, as it is transported down the pile, will be used to build the propagator we are looking for. The mth marked grain will be positioned, at some initial time, t_0^m, at an arbitrary cell i_m, chosen randomly from within a reduced number of cells near the top of the pile. The initial position of the mth grain is then $x_m(0) = i_m$; its depth in the i_m column, as measured from its top, will be initially set to $d^m(0) = uN_f$, where u is a random number uniformly distributed in [0,1]. As the sandpile is iterated, the position, x^m, and depth d^m of the marked grain

of sand will change. Their values, at the kth iteration, will be updated after finding out which of the following rules applies [33]:

(1) the current cell is stable and no grains of sand have been dropped on it in the previous driving phase;

then $d^m(k) = d^m(k-1)$; $x^m(k) = x^m(k-1)$;

(2) the current cell is stable, but N_b grains of sand have fallen on it in the previous driving phase;

then $d^m(k) = d^m(k-1) + N_b$; $x^m(k) = x^m(k-1)$;

(3) the current cell is stable, but the previous one is unstable and moves N_f grains over to the current cell;

then $d^m(k) = d^m(k-1) + N_f$; $x^m(k) = x^m(k-1)$;

(4) the current cell is stable, the previous one is unstable and, in the driving phase, N_b grains have fallen on the current cell;

then $d^m(k) = d^m(k-1) + N_f + N_b$; $x^m(k) = x^m(k-1)$;

(5) the current cell is unstable and N_f grains are thus moved to the following cell; no grains of sand have been dropped on the current cell in the driving phase;

then, if $d^m(k-1) \leqslant N_f \longrightarrow d^m(k) = uN_f$;
$x^m(k) = x^m(k-1) + 1$;
if $d^m(k-1) > N_f \longrightarrow d^m(k) = d^m(k) - N_f$;
$x^m(k) = x^m(k-1)$;

(6) the current cell is unstable and N_f grains are thus moved to the following cell; at the previous driving phase, N_b grains of rain have fallen on the current cell;

then, if $d^m(k-1) \leqslant N_f - N_b \longrightarrow d^m(k) = uN_f$;
$x^m(k) = x^m(k-1) + 1$;
if $d^m(k-1) > N_f - N_b \longrightarrow d^m(k) = d^m(k) - N_f + N_b$;
$x^m(k) = x^m(k-1)$.

The majority of these rules are rather self-explanatory. Basically, they state that, when it is time to move N_f particles to the next cell, our marked grain will be transported together with that bunch only if its depth in the cell is at most N_f. In that case, the marked grain of sand will reset its depth at the new cell to a new value, randomly chosen between 0 and N_f since u is a random number uniformly distributed in [0,1]. If the marked grain is, however, deeper than N_f, it remains at the current cell. In the (relatively rare) case that sand has been dropped during the previous driving phase on the same cell where the marked grain sits, the depth of the marked grain is increased by N_b.

Figure 4 shows the motion across the sandpile (size $L = 10\,000$, critical slope $Z_c = 200$, toppling size $N_f = 30$, rain probability $p_0 = 10^{-4}$, and rain size $N_b = 1$) of 10 marked grains of sand for the first 10^6 iterations. As can be appreciated, the grains alternate radial displacements when carried by a passing avalanche that appear as nearly horizontal segments (in fact, they are not exactly horizontal since particles advance one position per iteration; however, the scale of the temporal axis used in the figure makes them look so)−, with periods
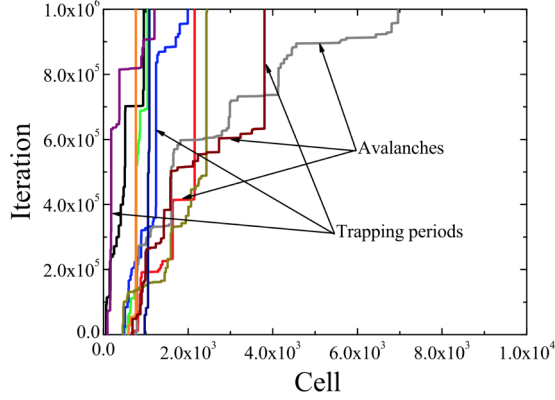
FIG. 4. Motion across the sandpile of size $L = 10\,000$ of 10 selected particles, with initial locations randomly chosen within the central half of the pile. The vertical parts of the trajectories correspond to periods in which the particle is at rest on some cell; the (almost) horizontal parts, to periods of time in which the particle is transported radially, carried away by passing avalanches.

of rest at the same cell, while the grain remains trapped there —that appear as vertical segments.

B. Propagator estimation in the running sandpile

The recorded positions of the marked grains of sand can be used to build a discrete version of the sandpile propagator. All that is needed is to calculate, at each iteration, the pdf of the particle displacements with respect to their respective initial locations, $p(\Delta x; k)$. By using relative displacements (from each initial location), we can seed many more marked grains than the N_f that would fit within the active narrow layer at a single location. We can now initialize up to N_f of them at as many cells as desired, which greatly improves the statistics. It must be said, though, that by doing so we have implicitly assumed that all these cells have similar dynamics. This is, to a great extent, the case for the running sandpile due to the uniformly spread random drive. Each marked grain will contribute with the displacement value $\Delta x^m(k) = x^m(k) - x^m(0)$ $(m = 1, \dots, N)$ at iteration k. Since $p(\Delta x; k)$ thus gives the probability of a particle having been displaced a distance Δx in a time k, averaged over its initial location, we can write that

$$p(\Delta x; k) \simeq \langle G(x_0 + \Delta x, k | x_0, 0) \rangle_{x_0}, \qquad (23)$$

which is the estimate of the propagator of the running sandpile we are looking for.

There are some limitations that, however, must be considered while estimating the propagator in this way. They are due to the unavoidable fact that each marked grain does eventually reach the end of the sandpile. Therefore, Eq. (23) should not be used beyond the typical number of iterations required for the closest marked particles to reach the pile edge. In addition, one also needs to consider that, since marked grains have been initialized at different locations in order to improve statistics, each one travels a different distance to reach the edge of the sandpile. To avoid possible distortions, contributions to Eq. (23) from any Δx larger than the minimum of these distances should also be disregarded.
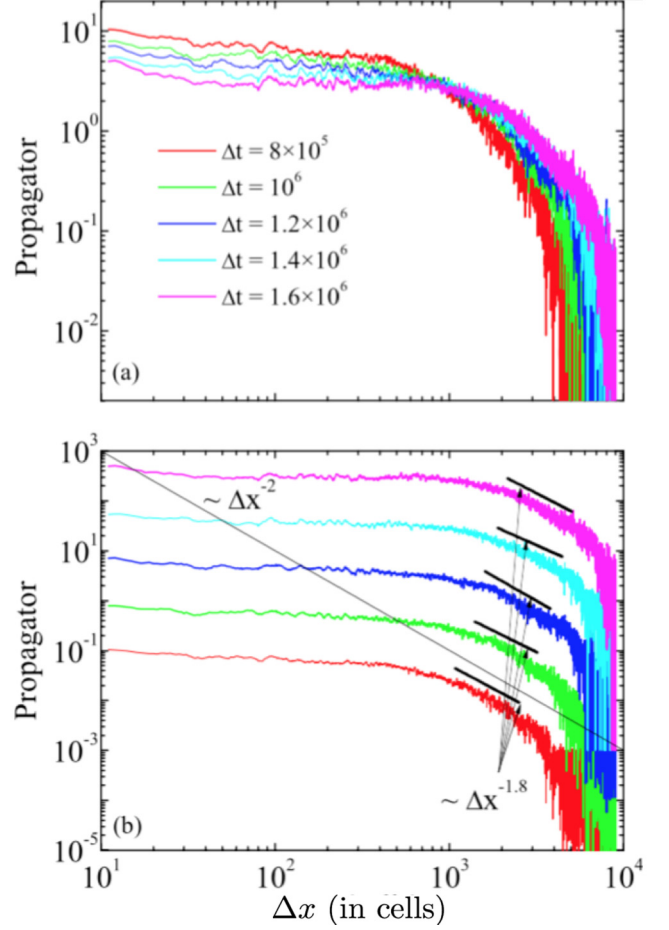

FIG. 5. (a) Sandpile propagator for times corresponding to $(0.8, 1.0, 1.2, 1.4, \text{and } 1.6) \times 10^6$ iterations using $10\,000$ tracer particles for the $L = 10\,000$ sandpile with $Z_c = 200$, $N_f = 30$, $N_b = 1$, and $P_0 = 10^{-4}$. In (b), the same propagators have been shifted to better appreciate the power-law regions scaling as $P(\Delta x) \sim \Delta x^{-1.8}$. The algebraic scaling Δx^{-2} is also shown (in black) to guide the eye.

Figure 5(a) shows snapshots of the sandpile propagator obtained at different times using $N = 10\,000$ marked grains, that were uniformly initialized at cells with $x^m(0) \leqslant x_{\max} = L/10 = 1000$ for any tracer $m \in [1, N]$ (note that $L = 10\,000$ for all these simulations). In Fig. 5(b) the same propagators have been shifted up (magenta and cyan) and down (red and green) to better appreciate the power-law regions where the corresponding fits have been performed. The propagators exhibit power-law regions beyond certain displacement values that are eventually replaced by exponential cutoffs due to finite-size effects. In particular, power-law scalings close to $p(\Delta x) \sim \Delta x^{-1.8}$ are apparent that become distorted at times of the order of 10^6 iterations and above. This number is of the order of the number of iterations required for a sizable amount of marked particles to have reached the sandpile edge. By using Eq. (20), we can thus infer a value $\alpha \sim 0.8$ for the spatial fractional exponent of the effective fractional transport model [Eq. (16)] for the running sandpile.

We estimate next the temporal fractional exponent by quantifying the initial growth [Eq. (21)] and later decay [Eq. (22)] of the propagator at a fixed location. In Fig. 6, its temporal
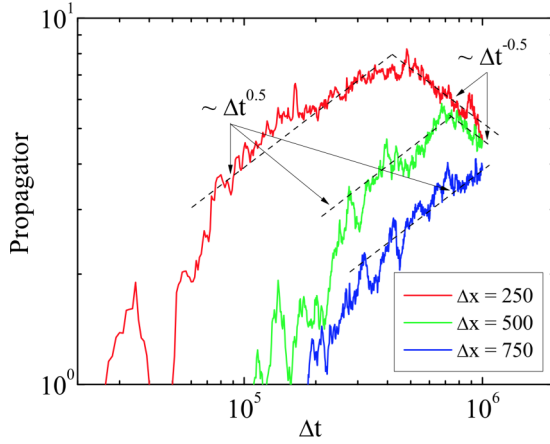
FIG. 6. Estimate of the evolution of the sandpile propagator at fixed positions, $\Delta x = 250$, $\Delta x = 500$, and $\Delta x = 750$, as a function of time using 10 000 tracer particles for the $L = 10\,000$ sandpile with $Z_c = 200$, $N_f = 30$, $N_b = 1$, and $P_0 = 10^{-4}$. As expected, the local value first grows and then decays algebraically as $P(\Delta t) \sim \Delta t^{\pm 0.5}$.

evolution is shown at three different fixed displacement values, $\Delta x = 250$, $\Delta x = 500$, and $\Delta x = 750$. For the smallest displacement, the propagator grows as $p(\Delta t) \sim \Delta t^{0.5}$ for $\Delta t < 4 \times 10^5$ and then decreases as $p(\Delta t) \sim \Delta t^{-0.5}$ for $\Delta t > 4 \times 10^5$. For $\Delta x = 500$, the propagator grows as $p(\Delta t) \sim \Delta t^{0.5}$ but for time lapses lasting double, $\Delta t < 8 \times 10^5$. Then decreases also as $p(\Delta t) \sim \Delta t^{-0.5}$ for $\Delta t > 8 \times 10^5$. Finally, for the largest displacement, the decay phase is, however, not seen within the 10^6 iterations considered. In fact, it would take approximately 1.6×10^6 iterations to appreciate the beginning of this phase for this displacement. Therefore, from Eqs. (21) and (22) we can infer a value $\beta \sim 0.5$ for the temporal exponent of the effective fractional transport model [Eq. (5)] for the running sandpile.

In order to increase our confidence in these exponent values, we have also estimated the pdfs of waiting times and jump sizes of the marked grains directly. To do it, we have
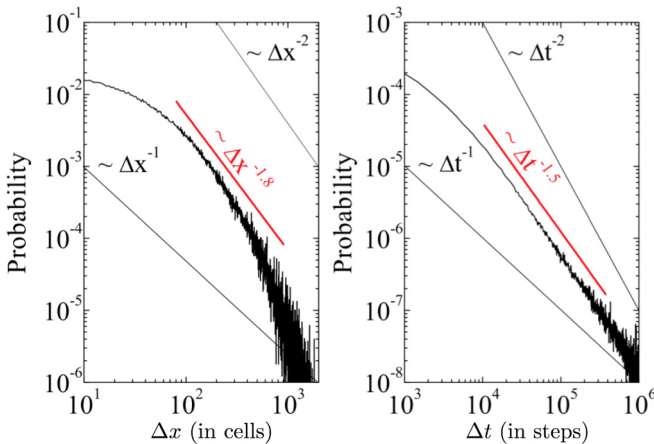

FIG. 7. Probability density functions for the jump sizes (left) and waiting times (right) of marked grains of sand moving across a running sandpile $L = 10\,000$ sandpile with $Z_c = 200$, $N_f = 30$, $N_b = 1$, and $P_0 = 10^{-4}$.

considered the (almost) horizontal marker displacements in Fig. 4 as the instantaneous jumps and the vertical segments as waiting times. Their pdfs are shown in Fig. 7. As can be seen, $p(\Delta x) \sim \Delta x^{-1.8}$ over sufficiently large values, before the appearance of the unavoidable exponential cutoff at the largest scales; on the other hand, $\psi(\Delta t) \sim \Delta t^{-1.5}$ over the mesorange scales. Therefore, these pdfs are consistent with the values $\alpha \sim 0.8$ and $\beta \sim 0.5$ that were obtained from the propagator analysis.

V. DISCUSSION

In the previous section, we have found that the long-range, large-scale features of transport across the running sandpile seem to be well modelled by Eq. (16) with $\alpha \sim 0.8$ and $\beta \sim 0.5$. The range of length scales over which the exponent α is well defined is, roughly, $\Delta x \in [10^2 - 10^3]$, well separated from the minimum (1) and maximum (10 000) sizes allowed in the sandpile ($L = 10\,000$), where finite-size effects are expected. The range of timescales over which β is well defined is longer, roughly $\Delta t \in [10^4 - 10^6]$. That is, much longer than the maximum duration avalanches can have in the sandpile, which is of the order of L. This suggests that the fact that exponent β is significantly smaller than 1 is needed to capture the long-term persistence that is associated to the evolution of the roughness of the sandpile height profile or, in other words, to the influence of the footprints left behind by previous avalanches on the future transport across the sandpile.

Another interesting point regards the aforementioned transport exponent, $H = \beta/\alpha$. As we mentioned previously, this transport exponent is often used when discussing symmetric transport [15,28]. Indeed, $H = 0.5$ is usually called a diffusive scaling, while $H > 0.5$ is referred to as superdiffusion, and $H < 0.5$ as subdiffusion. In the running sandpile, however, this interpretation is meaningless since the propagator for Eq. (16) is not only asymmetric but also fully biased towards the down-the-slope direction. Therefore, although one could still estimate this transport exponent to be $H \sim 0.62$, its value cannot be interpreted as indicative of superdiffusive transport taking place across the running sandpile. Indeed, H no longer quantifies how the propagator spreads with respect to its "center of mass" (as it does for symmetric motion) but how fast the "center of mass" moves down the slope (which, in a symmetric case, it does not).

Finally, we would like to make some comments regarding the practical use of Eq. (16) as an effective model for the running sandpile. The first comment is that the starting point of the spatial integral in Eq. (16) must be replaced by 0, the innermost sandpile position [or one could assume that $n(x,t) = 0$, $\forall x < 0$, at all times]. Second, the kernel of the Riesz-Feller integral might then need to be regularized to avoid a possible divergence of the fractional derivative at its starting point, $x = 0$, that might appear when imposing initial or boundary conditions expressed in terms of usual (i.e., integer) derivatives [34], as often happens in physical systems (see Appendix B). The regularization of fractional derivatives is a relatively standard practice in most applications of fractional transport equations. Many details about these procedures can be found in the literature [23].

VI. CONCLUSIONS

In this work, we have constructed an effective model for transport across the running sandpile cellular automaton based on fractional derivatives. The resulting transport equation [Eq. (16)] must be written in terms of fully asymmetric fractional derivatives both in space and time, due to the fully biased nature of sand motion in the sandpile, that only takes place down the slope. This is in contrast with more common applications of fractional transport equations that often describe systems in which unbiased, symmetric motion takes place, resulting in the use of symmetric fractional derivatives in space. This difference forces us to revise the interpretation of some of the exponents that characterize the model. We have also estimated the fractional exponents required to complete the effective model by using marked grains of sand as a diagnostic tool. We expect that this exercise might serve as a guide to address similar problems in more complicated systems such as, for example, the construction of reliable effective transport models for the radial transport of energy and particles out of fusion plasmas confined in tokamaks in near-marginal regimes [15].

APPENDIX A: STABLE LÉVY DISTRIBUTIONS

The Lévy family of pdfs comprises all the limit distributions that are strictly stable with respect to the sum of N independent and identically distributed random variables [30]. They can be defined in closed form only via their characteristic function (or Fourier transform):

$$L_{[\alpha,\lambda,\sigma]}(k) = \exp\left\{-\sigma^\alpha |k|^\alpha \left[1 - \frac{i\lambda k}{|k|} \tan\left(\frac{\pi\alpha}{2}\right)\right]\right\}, \quad (A1)$$

with the parameters varying in $\alpha \in (0,2]$, $|\lambda| \leqslant 1$, and $\sigma > 0$. Here $i = \sqrt{-1}$.

1. Meaning of parameters

Each parameter has a very different meaning. First, $|\lambda| \leqslant 1$ measures the asymmetry of the distribution since [30],

$$L_{[\alpha,\lambda,\sigma]}(y) = L_{[\alpha,-\lambda,\sigma]}(-y). \quad (A2)$$

If $\lambda = 0$, then the pdf is symmetric (and, for $\alpha = 1,2$, it is the only possible value). Second, α characterizes the tail behavior of the pdf. For $\alpha \neq 1$, it happens that [30],

$$L_{[\alpha,\lambda,\sigma]}(y) \sim \begin{cases} C_\alpha\left(\frac{1-\lambda}{2}\right)\sigma^\alpha |y|^{-(1+\alpha)}, & y \to -\infty \\ C_\alpha\left(\frac{1+\lambda}{2}\right)\sigma^\alpha |y|^{-(1+\alpha)}, & y \to +\infty \end{cases}, \quad (A3)$$

with the constant given by

$$C_\alpha = \frac{\alpha(\alpha - 1)}{\Gamma(2 - \alpha)\cos(\pi\alpha/2)}, \quad (A4)$$

with $\Gamma(x)$ being the usual Γ function. In the special case $\alpha = 1$, the Lévy pdf (known as a Cauchy pdf) decays as $L_{[1,0,\sigma]}(y) \sim (\sigma/\pi)|y|^{-2}$. Finally, σ is the scale parameter because [30],

$$L_{[\alpha,\lambda,\sigma]}(ay) = L_{[\alpha,\text{sgn}(a)\lambda,|a|\sigma]}(y). \quad (A5)$$

2. Extremal Lévy distributions

A Lévy distribution is called *extremal* if $\lambda = \pm1$ (this can only happen for $\alpha \neq 1,2$). According to Eq. (A3), the power-law decay is only observed for one of the two tails (for positive or negative y's) depending on the sign of λ, with the other tail decaying exponentially fast. Indeed, for $1 < \alpha < 2$, $\lambda = \pm1$ forces the tail for $y \to \mp\infty$ to decay exponentially. For $0 < \alpha < 1$ the extremal distribution becomes one sided [30]. That is, they are defined only for $y > 0$ if $\lambda = +1$ and for $y < 0$ if $\lambda = -1$. In that case, the exponential tail is found in the limit $y \to 0\pm$ for $\lambda \to \mp1$. A useful property of extremal Lévy distributions is that its Laplace transform is given by:

$$\tilde{L}_{[\alpha,1,\sigma]}(s) = \exp\left[-\frac{\sigma^\alpha}{\cos(\pi\alpha/2)}s^\alpha\right]. \quad (A6)$$

APPENDIX B: RIEMANN-LIOUVILLE FRACTIONAL DERIVATIVES

Riemann-Lioville (RL) fractional derivatives are integrod-ifferential operators that provide interpolants between derivatives of integer order [34].

1. Riemann-Liouville fractional derivatives

The left-sided RL fractional derivative of order $p > 0$ of a function $f(t)$ is defined as [34]

$$_aD_t^p f(t) \equiv \frac{1}{\Gamma(k - p)} \frac{d^k}{dt^k} \int_a^t (t - \tau)^{k-p-1} f(\tau)d\tau, \quad (B1)$$

where the integer k satisfies that $k - 1 \leqslant p < k$. For $p = n$, the RL fractional derivative reduces to the standard derivative of order n. Right-sided RL fractional derivatives can also be defined:

$$_bD_t^p f(t) \equiv \frac{1}{\Gamma(k - p)} \frac{d^k}{dt^k} \int_t^b (\tau - t)^{k-p-1} f(\tau)d\tau. \quad (B2)$$

Their properties are analogous to the left-sided counterpart.

RL fractional derivatives have interesting but somewhat not intuitive properties. The most striking property is probably that the fractional derivative of a constant function is not zero. Indeed, using the fact that the derivative of a power law can be

calculated to be [30] ($p > 0$, $\nu > -1$, $t > 0$):

$$_aD_t^p(t-a)^\nu = \frac{\Gamma(1+\nu)}{\Gamma(1+\nu-p)}(t-a)^{\nu-p}, \qquad \text{(B3)}$$

it is clear that choosing $\nu = 0$ does not yield a constant, but $(t-a)^{-p}/\Gamma(1-p)$.

RL fractional derivatives can be combined with other derivatives (fractional or integer). But the combinations are not always simple. For instance, the action of normal derivatives on RL fractional derivatives is

$$\frac{d^m}{dt^m}\,_aD_t^p f(t) =\,_aD_t^{p+m} f(t). \qquad \text{(B4)}$$

For the right-side RL derivatives, this property becomes

$$(-1)^m\frac{d^m}{dt^m}\,^bD_t^p f(t) =\,^bD_t^{p+m} f(t). \qquad \text{(B5)}$$

However, the action of the RL fractional derivative on a normal derivative is much more complicated [30].

Relatively simple expressions exist for the Laplace transform of the left-sided RL fractional derivative of order p if the starting point is $a = 0$:

$$L\left[_0D_t^p \cdot f(t)\right] = s^p \tilde{f}(s) - \sum_{j=0}^{k-1} s^j \left[_0D_t^{p-j-1} \cdot f(t)\right]_{t=0}. \qquad \text{(B6)}$$

This expression is very reminiscent of the one for normal derivatives. Similarly, the Fourier transform of the left-sided RL fractional derivative satisfies a very simple relation when the starting point is $a = -\infty$:

$$\text{F}\left[_{-\infty}D_t^p \cdot f(t)\right] = (i\omega)^p \hat{f}(\omega). \qquad \text{(B7)}$$

For the right-sided fractional integral with ending point $b = \infty$, the Fourier transform satisfies

$$\text{F}\left[^\infty D_t^p \cdot f(t)\right] = (-i\omega)^p \hat{f}(\omega). \qquad \text{(B8)}$$

Finally, it is worth mentioning that the left- (right-) sided fractional derivative of a function $f(x)$ may exhibit a divergence at their start (end) point when one prescribes the values of this function or its integer derivatives at the start (end) point (as it is often done in many applications, where initial value or boundary value problems often appear). This can be made apparent, for instance, by calculating the fractional derivative of a regular function by means of its Taylor expansion. In the case in which $0 < \alpha < 1$, it becomes [23]

$$_aD_t^\alpha f(x) = \frac{1}{\Gamma(1-a)}\frac{f(a)}{(x-a)^\alpha}$$
$$+ \sum_{k=0}^\infty \frac{f^{(k+1)}(a)}{\Gamma(k+2-\alpha)}(x-a)^{k+1-\alpha}. \qquad \text{(B9)}$$

This expression is clearly divergent at $x = a$ if $f(a) \neq 0$. A similar expression can be obtained for $1 < \alpha < 2$. In that case,

$$_aD_t^\alpha f(x) = \frac{1}{\Gamma(1-a)}\frac{f(a)}{(x-a)^\alpha} + \frac{1}{\Gamma(2-a)}\frac{f'(a)}{(x-a)^{\alpha-1}}$$
$$+ \sum_{k=0}^\infty \frac{f^{(k+2)}(a)}{\Gamma(k+3-\alpha)}(x-a)^{k+2-\alpha} \qquad \text{(B10)}$$

that is divergent at $x = a$ if either $f(a) \neq 0$ or $f'(a) \neq 0$. These divergences can be avoided if one prescribes the values of fractional derivatives of the function at the start (end) point instead. However, this is usually difficult to justify physically in most situations [34]. For that reason, regularization techniques are often used to avoid these divergences in practical applications, as it has been widely described in the literature [23].

APPENDIX C: THE RIESZ-FELLER FRACTIONAL DERIVATIVES

The Riesz fractional derivative of order α is defined by the integral:

$$\frac{\partial^\alpha f}{\partial|x|^\alpha} := -\frac{1}{2\Gamma(\alpha)\cos(\alpha\pi/2)}\int_{-\infty}^\infty dx' \frac{f(x')}{|x-x'|^{\alpha+1}}. \qquad \text{(C1)}$$

The most remarkable property of this derivative has to do with its Fourier transform that satisfies [35]:

$$\text{F}\left[\frac{\partial^\alpha f}{\partial|x|^\alpha}\right] = -|k|^\alpha \hat{f}(k). \qquad \text{(C2)}$$

Using now the complex identity ($i = \sqrt{-1}$),

$$(ik)^\alpha + (-ik)^\alpha = 2\cos\left(\frac{\pi\alpha}{2}\right)|k|^\alpha, \qquad \text{(C3)}$$

it is very easy to prove that the Riesz derivative can also be expressed as a symmetric sum of two RL fractional derivatives (one left-sided, one right-sided) of order α [30],

$$\frac{\partial^\alpha f}{\partial|x|^\alpha} = -\frac{1}{2\Gamma(\alpha)\cos(\alpha\pi/2)}\left[_{-\infty}D_x^\alpha + {}^\infty D_x^\alpha\right]. \qquad \text{(C4)}$$

An asymmetric version of the Riesz-Feller derivative also exists [36]. It is often referred to as the Riesz-Feller fractional derivative of order α with asymmetry parameter $|\lambda| \leqslant 1$. It is more easily defined through its Fourier transform, that is,

$$\text{F}\left[\frac{\partial^{\alpha,\lambda} f}{\partial|x|^{\alpha,\lambda}}\right] = -|k|^\alpha\left[1 - i\lambda\frac{|k|}{k}\tan\left(\frac{\alpha\pi}{2}\right)\right]\hat{f}(k). \qquad \text{(C5)}$$

For $\lambda = 0$, the standard symmetric Riesz derivative is recovered. The asymmetric Riesz-Feller derivative can also be expressed as an asymmetric sum of two RL fractional derivatives of order α [37]:

$$\frac{\partial^{\alpha,\lambda} f}{\partial|x|^{\alpha,\lambda}} = -\frac{1}{2\Gamma(\alpha)\cos(\alpha\pi/2)}$$
$$\times\left[c_-(\alpha,\lambda)_{-\infty}D_x^\alpha f + c_+(\alpha,\lambda)^\infty D_x^\alpha f\right], \qquad \text{(C6)}$$

with the $c_\pm$ coefficients being defined as

$$c_\pm(\alpha,\lambda) := \frac{1 \mp \lambda}{1 + \lambda\cos\left(\frac{\alpha\pi}{2}\right)}. \qquad \text{(C7)}$$

Thus, in the limit of $\lambda = 1$, only the left-sided RL derivative $_{-\infty}D_x^\alpha$ remains, while for $\lambda = -1$, only the right-side RL derivative $^\infty D_x^\alpha$ does.

[1] P. Bak, C. Tang, and K. Wiesenfeld, Phys. Rev. Lett. **59**, 381 (1987).

[2] E. T. Lu and R. J. Hamilton, Astroph. J. **380**, L89 (1991).

[3] B. E. Shaw, J. M. Carlson, and J. S. Langer, J. Geophys. Res. **97**, 479 (1992).

[4] B. Drossel and F. Schwabl, Phys. Rev. Lett. **69**, 1629 (1992).

[5] P. Bak and K. Sneppen, Phys. Rev. Lett. **71**, 4083 (1993).

[6] S. Mineshige, M. Takeuchi, and H. Nishimori, Astroph. J. **435**, L125 (1994).

[7] T. Nagatani, Physica A **218**, 145 (1995).

[8] S. Field, J. Witt, F. Nori, and X. Ling, Phys. Rev. Lett. **74**, 1206 (1995).

[9] S. Nagel, Rev. Mod. Phys. **64**, 321 (1992).

[10] J. Feder, Fractals **03**, 431 (1995).

[11] L. P. Kadanoff, S. R. Nagel, L. Wu, and S.-M. Zhou, Phys. Rev. A **39**, 6524 (1989).

[12] T. Hwa and M. Kardar, Phys. Rev. A **45**, 7002 (1992).

[13] D. E. Newman, B. A. Carreras, P. H. Diamond, and T. S. Hahm, Phys. Plasmas **3**, 1858 (1996).

[14] R. Sanchez, D. E. Newman, and B. A. Carreras, Nucl. Fusion **41**, 247 (2001).

[15] R. Sanchez and D. E. Newman, Plasma Phys. Control. Fusion **57**, 123002 (2015).

[16] P. H. Diamond and T. S. Hahm, Phys. Plasmas **2**, 3640 (1995).

[17] B. A. Carreras *et al.*, Phys. Plasmas **3**, 2903 (1996).

[18] E. J. Doyle *et al.*, Nucl. Fusion **47**, S18 (2007).

[19] B. A. Carreras, V. E. Lynch, and G. M. Zaslaysky, Phys. Plasmas **8**, 5096 (2001).

[20] B. Ph. van Milligen, R. Sanchez, and B. A. Carreras, Phys. Plasmas **11**, 2272 (2004).

[21] D. del-Castillo-Negrete, B. A. Carreras, and V. E. Lynch, Phys. Plasmas **11**, 3854 (2004).

[22] R. Sanchez, B. A. Carreras, and B. Ph. van Milligen, Phys. Rev. E **71**, 011111 (2005).

[23] D. del-Castillo-Negrete, Phys. Plasmas **13**, 082308 (2006).

[24] M. V. Medvedev and P. H. Diamond, Phys. Rev. E **58**, 6824 (1998).

[25] J. A. Mier, R. Sanchez, and D. E. Newman, Phys. Rev. E **94**, 022128 (2016).

[26] R. A. Woodard *et al.*, Physica A **373**, 215 (2007).

[27] E. W. Montroll and G. Weiss, J. Math. Phys. **6**, 167 (1965).

[28] R. Metzler and J. Klafter, Phys. Rep. **339**, 1 (2000).

[29] M. M. Meerschaert and P. Straka, Ann. Probab. **42**, 1699 (2014).

[30] G. Samorodnitsky and M. S. Taquu, *Stable Non-Gaussian Random Processes* (Chapman & Hall, New York, 1994).

[31] M. M. Meerschaert and A. Sikorskii. *Stochastic Models for Fractional Calculus* (De Gruyter, Berlin, 2012).

[32] A. Saichev and G. M. Zaslaysky, Chaos **7**, 753 (1997).

[33] B. A. Carreras, V. E. Lynch, D. E. Newman, and G. M. Zaslavsky, Phys. Rev. E **60**, 4770 (1999).

[34] I. Podlubny, *Fractional Differential Equations* (Academic Press, New York, 1998).

[35] S. G. Samko, A. A. Kilbas, and O. I. Marichev, *Fractional Integrals and Derivatives: Theory and Applications* (Gordon & Breach, New York, 1993).

[36] W. Feller, *Introduction to Probability Theory and Applications* (Wiley, New York, 1968).

[37] R. Gorenflo *et al.*, Chem. Phys. **284**, 521 (2002).